Low-Temperature approach to highly emissive copper indium sulfide colloidal nanocrystals and their bioimaging applications

Yu, Kui; Ng, Peter; Ouyang, Jianying; Zaman, Md. Badruz; Abulrob, Abedelnasser; Baral, Toya Nath; Fatehi, Dorothy; Jakubek, Zygmunt J.; Kingston, David; Wu, Xiaohua; Liu, Xiangyang; Hebert, Charlie; Leek, Donald M.; Whitfield, Dennis M.

National Research Council Canada   Conseil national de recherches Canada

Canada

Low-Temperature Approach to Highly Emissive Copper Indium Sulfide Colloidal Nanocrystals and Their Bioimaging Applications

Kui Yu,*[†] Peter Ng,[†] Jianying Ouyang,[†] Md. Badruz Zaman,[†,‡,§] Abedelnasser Abulrob,[‡]
Toya Nath Baral,[‡] Dorothy Fatehi,[‡] Zygmunt J. Jakubek,[†] David Kingston,[⊥] Xiaohua Wu,[⊥]
Xiangyang Liu,[†] Charlie Hebert,[†] Donald M. Leek,[†] and Dennis M. Whitfield*[‡]

[†]Emerging Technologies, [‡]Life Sciences, and [⊥]Engineering, National Research Council of Canada, Ottawa, Ontario, K1A 0R6, Canada

S *Supporting Information*

ABSTRACT: We report our newly developed low-temperature synthesis of colloidal photoluminescent (PL) $CuInS_2$ nanocrystals (NCs) and their in vitro and in vivo imaging applications. With diphenylphosphine sulphide (SDPP) as a S precursor made from elemental S and diphenylphosphine, this is a noninjection based approach in 1-dodecanethiol (DDT) with excellent synthetic reproducibility and large-scale capability. For a typical synthesis with copper iodide (CuI) as a Cu source and indium acetate $(In(OAc)_3)$ as an In source, the growth temperature was as low as 160 °C and the feed molar ratios were 1Cu-to-1In-to-4S. Amazingly, the resulting

$CuInS_2$ NCs in toluene exhibit quantum yield (QY) of ~23% with photoemission peaking at ~760 nm and full width at half maximum (FWHM) of ~140 nm. With a mean size of ~3.4 nm (measured from the vertices to the bases of the pyramids), they are pyramidal in shape with a crystal structure of tetragonal chalcopyrite. In situ ^{31}P NMR (monitored from 30 °C to 100 °C) and in situ absorption at 80 °C suggested that the Cu precursor should be less reactive toward SDPP than the In precursor. For our in vitro and in vivo imaging applications, $CuInS_2$/ZnS core−shell QDs were synthesized; afterwards, dihydrolipoic acid (DHLA) or 11-mercaptoundecanoic acid (MUA) were used for ligand exchange and then bio-conjugation was performed. Two single-domain antibodies (sdAbs) were used. One was 2A3 for in vitro imaging of BxPC3 pancreatic cancer cells. The other was EG2 for in vivo imaging of a Glioblastoma U87MG brain tumour model. The bioimaging data illustrate that the $CuInS_2$ NCs from our SDPP-based low-temperature noninjection approach are good quality.

KEYWORDS: $CuInS_2$ nanocrystals, quantum dots, diphenylphosphine sulphide, in vitro imaging, in vivo imaging
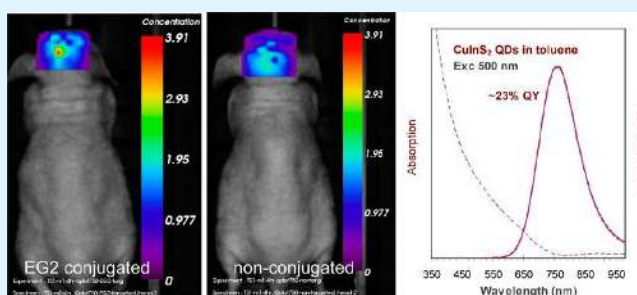
1. INTRODUCTION

Colloidal semiconductor nanocrystals (NCs), such as I−III−VI $CuInS_2$ NCs which are cadmium-free and lead-free, have attracted significant attention for their potential in a wide range of applications.[1−12] With a bulk exciton Bohr radius of ~4.1 nm, $CuInS_2$ NCs could exhibit significant quantum confinement effect (QCE) when they are smaller than ~8 nm; furthermore, with a bulk direct bandgap of ~1.5 eV (827 nm), $CuInS_2$ NCs could be tuned to emit from the visible to near-infrared (NIR) spectral range. Recently, in vivo imaging of mice sentinel lymph node suggested that $CuInS_2$/ZnS NCs exhibited reduced toxicity, as compared to CdTeSe/CdZnS QDs.[8] Thus, with high absorption coefficients, $CuInS_2$ NCs are good candidates as fluorescent contrast agents for biolabeling/imaging.[7−12]

Various synthetic methods to emissive $CuInS_2$ NCs have been reported and are summarized in Table S1 in the Supporting Information.[7,13−25] These methods required reaction temperatures as high as 200−240 °C, and the resulting $CuInS_2$ NCs typically exhibit emission quantum yields (QYs) ≤

10%. Thus, there is a significant demand for the development of lower temperature synthesis of brighter $CuInS_2$ NCs. Diphenylphosphine (DPP), a commercially available secondary phosphine, has been applied actively in our laboratories and a few other groups to promote various semiconductor NCs including PbSe,[26−29] PbSeS,[30−32] PbSeTe,[32] PbSTe,[32] ZnSe,[33] ZnSeS,[34] CdS,[35] and CdSe,[36,37] with high particle yield and high synthetic reproducibility via a noninjection-based approach in 1-octadecene (ODE) at low temperature.

Herein, we report our newly developed, low-temperature, non-injection-based one-pot approach to highly-photoluminescent $CuInS_2$ NCs. The synthesis was carried out in 1-dodecanethiol (DDT, $CH_3(CH_2)_{11}SH$, RSH) instead of ODE, with diphenylphosphine sulfide (SDPP) as a sulfur
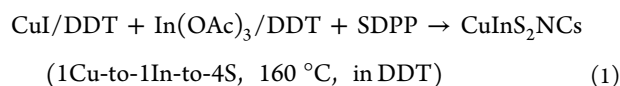
precursor made from elemental S and DPP. To the best of our knowledge, the present study is the first using SDPP to synthesize $CuInS_2$ NCs at temperature as low as 160 °C. Extensive optimization of experimental parameters such as various Cu (I), Cu (II), and In (III) source compounds, Cu-to-In-to-SDPP feed molar ratios, SDPP concentrations, and alternative solvents/ligands (including ODE, oleic acid (OA), and oleylamine (OLA)) suggested an optimal approach in DDT with the feed molar ratio of 1CuI-to-1In(OAc)$_3$-to-4SDPP, as shown by eq 1. The resulting $CuInS_2$ NCs dispersed in toluene exhibited QY as high as 23%. Structural and compositional characterizations by transmission electron microscopy (TEM), X-ray diffraction (XRD), X-ray photo-electron spectroscopy (XPS), and energy-dispersive X-ray spectroscopy (EDX) were performed. The resulting $CuInS_2$ NCs are gradiently-alloyed with Cu locating more on the inner part and In more on the outer layer. Both in situ high-resolution ^{31}P NMR with ^{1}H decoupling and in situ absorption measurements testify that the reactivity of CuI/DDT toward SDPP in DDT is lower than that of In(OAc)$_3$/DDT. Furthermore, in situ high-resolution ^{31}P NMR suggests that the combination of Cu−S and In−S monomers leads to nucleation/growth of the alloyed $CuInS_2$ NCs, as shown in Scheme 1.

$$CuI/DDT + In(OAc)_3/DDT + SDPP \rightarrow CuInS_2 NCs$$

$$(1Cu\text{-}to\text{-}1In\text{-}to\text{-}4S, \ 160\ °C, \ in\ DDT) \tag{1}$$

Scheme 1. Schematic Drawing of the Formation of the $CuInS_2$ NCs via the Combination of the Two Monomers of Cu−S and In−S. The Valence of Cu and In Is Not Addressed Here. The Combination of Monomers Leading to Nucleation and Growth Was Proposed before for Binary and Ternary NC Systems[26,27,34,37]

$$CuI/DDT + SDPP \rightarrow Cu\text{-}S\ monomers$$

$$In(OAc)_3/DDT + SDPP \rightarrow In\text{-}S\ monomers$$

$$Cu\text{-}S\ monomers + In\text{-}S\ monomers \rightarrow nucleation/growth\ CuInS_2\ NCs$$
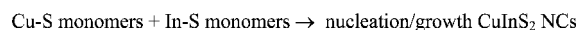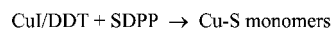
The developed $CuInS_2$ NCs were applied to in vitro and in vivo imaging, with well-established cancer model systems. After coating with a ZnS shell, the resulting $CuInS_2$/ZnS NCs were transferred into water and then bio-conjugated with single domain antibodies (sdAbs). As outlined in our previous papers,[38,39] sdAbs, such as EG2 and 2A3, have favorable chemical and physical properties for QD-based bio-imaging applications. EG2 was raised against the epidermal growth factor receptor (EGFR), which is a known tumor marker. 2A3 was raised against carcinoembryonic antigen-related cell adhesion molecule 6 (CEACAM6), a known tumor associated antigen of pancreatic cancer.[40,41] In the present study, pancreatic cancer cell lines were used to assess in vitro imaging with QD-2A3 bio-conjugates, and a Glioblastoma U87MG delta EGFR model for in vivo imaging of brain cancer in mice with QD-EG2 bioconjugates.

2. RESULTS AND DISCUSSION

Figure 1 shows the optical properties of one $CuInS_2$ NC ensemble from our low-temperature noninjection approach shown in eq 1. The growth was at 160 °C for 120 min, with a [Cu + In] concentration of 106 mmol/kg in DDT and 1CuI/DDT-to-1In(OAc)$_3$/DDT-to-4SDPP feed molar ratios. The as-synthesized sample emitted at 768 nm with its photo-luminescent (PL) QY in toluene estimated to be ~23.2% (based on dye Oxazine 170 in ethanol with 60% QY).[42] The $CuInS_2$ NCs exhibited good storage stability, as monitored after dark storage at −30 °C for ~3 months.

Figure S1A in the Supporting Information shows the temporal evolution of the optical properties of the as-synthesized $CuInS_2$ NCs from another batch of the eq 1 approach with the same 1CuI/DDT-to-1In(OAc)$_3$/DDT-to-4SDPP feed molar ratios but a [Cu + In] concentration of 72 mmol/kg in DDT. Eleven samples were taken from 50−160 °C, and the nucleation/growth took place at temperature lower than 50 °C. A persistent increase in photoemission QY is worthy of notice, as demonstrated in Figure S1A (bottom left) in the Supporting Information. Such an increase from Sample 5 (120 °C/15 min) to Sample 11 (160 °C/120 min) is similar to what was observed during the growth of $Zn_xCd_{1-x}S$ gradiently alloyed QDs[43] and CdTe/CdSe core−shell QDs.[44] Figure S1B in the Supporting Information demonstrates the good synthetic
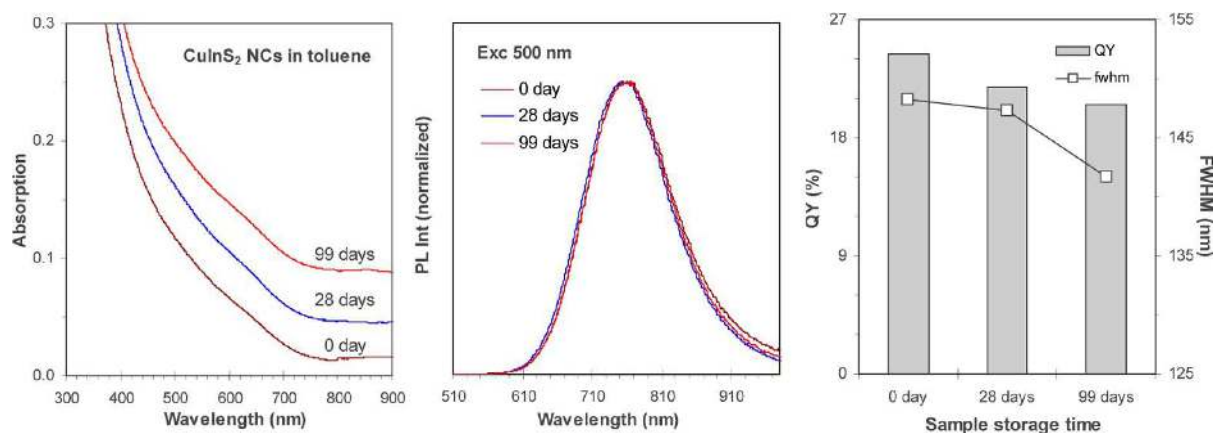
Figure 1. Optical properties of the resulting $CuInS_2$ NCs from the eq 1 approach with [Cu + In] 106 mmol/kg in DDT and 1CuI-to-1In(OAc)$_3$-to-4SDPP feed molar ratios. The growth was at 160 °C for 120 min, and the PL QY was estimated to be ~23% for the as-synthesized NCs. The absorption (left, offset) and emission (middle, normalized) measurements were performed at 0 day (as-synthesized), and after 28 and 99 days storage in the dark at −30 °C, with one identical sample concentration of 3 μL of the crude reaction mixture dispersed in 1.0 mL of toluene.
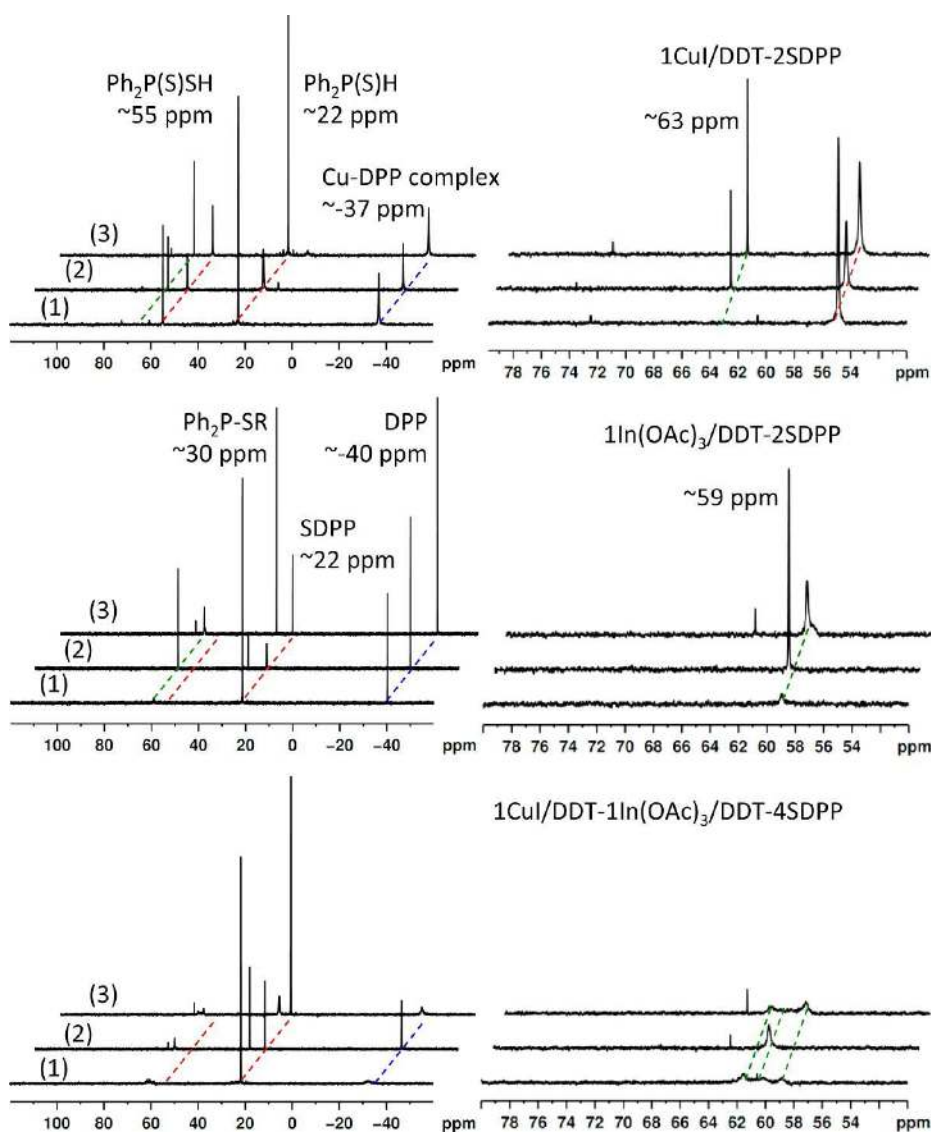
Figure 2. In situ ^{31}P NMR with ^{1}H decoupling of three reactions of 1CuI/DDT-2SDPP with [Cu] ~74 mmol/kg (top), 1In(OAc)$_3$/DDT-2SDPP with [In] ~21 mmol/kg (middle), and 1CuI/DDT-1In(OAc)$_3$/DDT-4SDPP with [Cu + In] ~38 mmol/kg (bottom). The spectra (left) were collected when the temperature was increased from 30 °C (1) to 100 °C (2) and back to 30 °C (3), as indicated. The regions of 50−80 ppm in the right panel display probable Cu−S and In−S complexes formed.

reproducibility with the comparison of the two synthetic batches, namely the relatively large-scale batch shown in Figure 1 and the relatively small-scale batch shown in Figure S1A in the Supporting Information. The former was 1.5 times of the [Cu + In] concentration and 3.5 times of the volume of the latter. Although two samples were taken from the former and 11 samples from the latter, both the two samples with 120 min growth at 160 °C exhibited emission peaking at ~760 nm with ~144 nm FWHM.

It should be pointed out that, for the eq 1 approach, the Cu and In precursors could be in the form of Cu-SR and [In]-(SR)$_n$ (n = 1−3, RSH = DDT), respectively, after the two mixtures of CuI and DDT, and In(OAc)$_3$ and DDT were kept at 65 °C under a strong vacuum (~50 mTorr) for at least 1 h. We symbolize preferably CuI/DDT as the Cu precursor and In(OAc)$_3$/DDT as the In precursor, due to the possible presence of I$^-$ and OAc$^-$ without purification. Furthermore, being a sulphur precursor, SDPP is much more reactive than DDT, as evidenced by the substantial decrease in nucleation

temperature. As shown in Figure S1C (top left) in the Supporting Information, with DDT as a sulphur source and with CuI and In(OAc)$_3$ as the respective Cu and In sources, the nucleation of CuInS$_2$ NCs in ODE took place at ~180 °C. Therefore, the optimal growth temperature with SDPP as the sulfur source could be reduced to 160 °C, which is appreciably lower than the typical CuInS$_2$ NC growth temperature of 200−240 °C.[7,13−25]

Figure 2 presents ^{31}P NMR spectra with ^{1}H decoupling in situ collected from three reaction mixtures of 1CuI/DDT + 2SDPP (top), 1In(OAc)$_3$/DDT + 2SDPP (middle), and 1CuI/DDT + 1In(OAc)$_3$/DDT + 4SDPP in DDT (bottom). 85% H$_3$PO$_4$ was used as an external standard and the spectra were collected when the temperature was increased from 30 °C (1) to 100 °C (2) and back to 30 °C (3). As shown in the top-right part of Figure S2 in the Supporting Information, three phosphorous-containing species were readily detected in the SDPP stock solution made from a mixture of 1S-to-1DPP (feed molar ratio); they are SDPP (Ph$_2$P(S)H, ~22 ppm)[34,35] as a
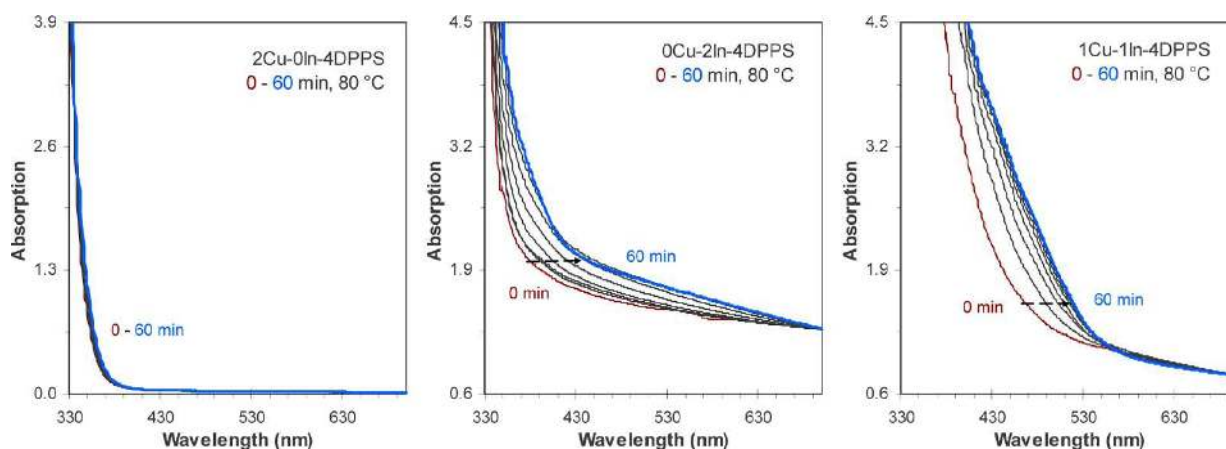
Figure 3. In situ observation of the nucleation/growth of the NCs from three batches at 80 °C. With a [Cu + In] concentration of 10 mmol/kg, the three batches are 2CuI/DDT-4SDPP (left), 2In(OAc)$_3$/DDT-4SDPP (middle), and 1CuI/DDT-1In(OAc)$_3$/DDT-4SDPP (right). The absorption spectra were collected with 5 min intervals, and the purple and blue spectra stand for the growth periods of 0 and 60 min, respectively.

major component (76%), diphenyldithiophosphinic acid (Ph$_2$P(S)SH, ~55 ppm)[34,45] as a minor component (11%), together with DPP (13%, approximately −40 ppm).[26,27,29] Also, trace amounts of one unknown species (~61 ppm) and Ph$_2$P(S)OH (~73 ppm)[46] were detected, the latter of which could be the result of the oxidation of Ph$_2$P(S)H.

As shown in the top panel of Figure 2, the 1CuI/DDT-2SDPP reaction mixture at 30 °C (1) exhibits appreciable peaks at −36.9 ppm (a Cu-DPP complex),[47,48] 22.8 ppm (Ph$_2$P(S)-H), 54.9 ppm (Ph$_2$P(S)SH), 60.6 ppm (the unknown from the SDPP stock solution), and 72.5 ppm (Ph$_2$P(S)OH). The formation of the Cu-DPP complex is supported by two mixtures of 1CuI/DDT-to-3DPP and 1CuI/DDT-to-6DPP with low-temperature in situ ^{31}P NMR measurements which are presented in the left panel of Figure S2A in the Supporting Information. The two spectra (1) and (3) collected at 30 °C before and after heating to 100 °C illustrate the decrease of Ph$_2$P(S)SH with a little change of Ph$_2$P(S)H, and the appearance and increase of the ~63 ppm peak (CuS$_2$PPh$_2$).[49,50]

As shown in middle panel of Figure 2, the In(OAc)$_3$/DDT-2SDPP reaction mixture at 30 °C (1) displays three noticeable peaks at −40.3 ppm (DPP), 21.3 ppm (Ph$_2$P(S)H), and 58.9 ppm ([In]-(S$_2$PPh$_2$)$_x$ with $1 \leq x < 3$). The chemical shift of In(S$_2$PPh$_2$)$_3$ in CDCl$_3$ was reported to be δ = 68.9 ppm.[51] The sharp DPP (approximately −40 ppm) peak suggests the absence of an In-DPP complex. The disappearance of the peaks of ~73 ppm (Ph$_2$P(S)OH), ~61 ppm, and ~55 ppm (Ph$_2$P(S)SH), together with the decrease of the ~23 ppm peak (Ph$_2$P(S)H), indicates the high In(OAc)$_3$/DDT reactivity. The increase in the peak of ~59 ppm and the DPP peak of ~40 ppm stands for the formation of [In]-(S$_2$PPh$_2$)$_x$ accompanied by the release of DPP, together with an increase of a substantial peak at ~29.5 ppm, which is assigned to Ph$_2$P-SR.[52]

The above ^{31}P NMR study shown in Figure 2 illustrates that the reactivity of In(OAc)$_3$/DDT is higher than that of CuI/DDT, which could be explained by the hard-soft-acid-base (HSAB) principle.[53] Cu^{1+} is considered as a soft acid, In^{3+} a hard acid, and DDT a soft base.[14,18] Accordingly, the Cu-SR bond should be stronger than the In-SR bond, and CuI/DDT is less reactive than In(OAc)$_3$/DDT. Such reactivity difference could be demonstrated by in situ absorption shown in Figure 3, where nucleation did not take place for the 2CuI/DDT-4SDPP mixture at 80 °C (left), but did for the 2In(OAc)$_3$/DDT-

4SDPP (middle) and 1CuI/DDT-1In(OAc)$_3$/DDT-4SDPP (right) mixtures at 80 °C.

As shown in the bottom panel of Figure 2, the 1CuI/DDT-1In(OAc)$_3$/DDT-4SDPP reaction mixture seems to be a simple superimposition of the 1CuI/DDT-2SDPP (top) and In(OAc)$_3$/DDT-2SDPP (middle) reactions. Spectrum (3) discloses phosphorus-containing species including CuS$_2$PPh$_2$ (~62 ppm), In(S$_2$PPh$_2$)$_x$ (~59 ppm), Ph$_2$P-SR (~29 ppm), Ph$_2$P(S)H (~22 ppm), and the Cu-DPP complex (~-34 ppm). The absence of addition reactions conveys essential information on the probable formation mechanism of the CuInS$_2$ alloyed NCs, namely the combination of individual Cu−S and In−S monomers formed leading to nucleation/growth shown in Scheme 1.[27] See the absorption and emission of the resulting CuInS$_2$ NCs shown in the bottom-right part of Figure S2 in the Supporting Information; the ready formation of the CuInS$_2$ NCs at low temperatures is worthy of notice. At the same time, the relative peak shapes of approximately −37 ppm in the top and bottom of Figure 2 of Spectrum (2) collected at 100 °C and Spectrum (3) at 30 °C are interesting. The significant difference of approximately −37 ppm at 30 °C of the two Spectra (3) indicates two different environments, where the phosphorous-containing species moved faster in Figure 2, top (without the formation of nanoparticles) than in Figure 2, bottom (with the formation of nanoparticles). At 100 °C, the environment effects decreased with two sharp approximately −37 ppm peaks in the top and bottom of Figure 2. The sharpness of NMR peaks is sensitive to environment and conformational exchange.

To explore the growth, we performed another batch that was similar to that shown in Figure 1 but with [Cu + In] 141 mmol/kg, and samples were taken at 100 °C/15 min (Sample 1), 160 °C/15 min (Sample 2), and 160 °C/120 min (Sample 3). The optical properties of the three samples are presented in Figure S4A in the Supporting Information, together with dark-field TEM images in Figure S4B in the Supporting Information. Figure 4, top, shows the powder X-ray diffraction (XRD) patterns of the three samples purified, together with that of bulk CuInS$_2$. The CuInS$_2$ NCs seem to have a tetragonal chalcopyrite crystal structure, as suggested by the XRD pattern and the pyramidal shape revealed by TEM (see Figure S1B in the Supporting Information). Along the growth from 100 °C to 160 °C, the XRD peaks become narrower, indicating an
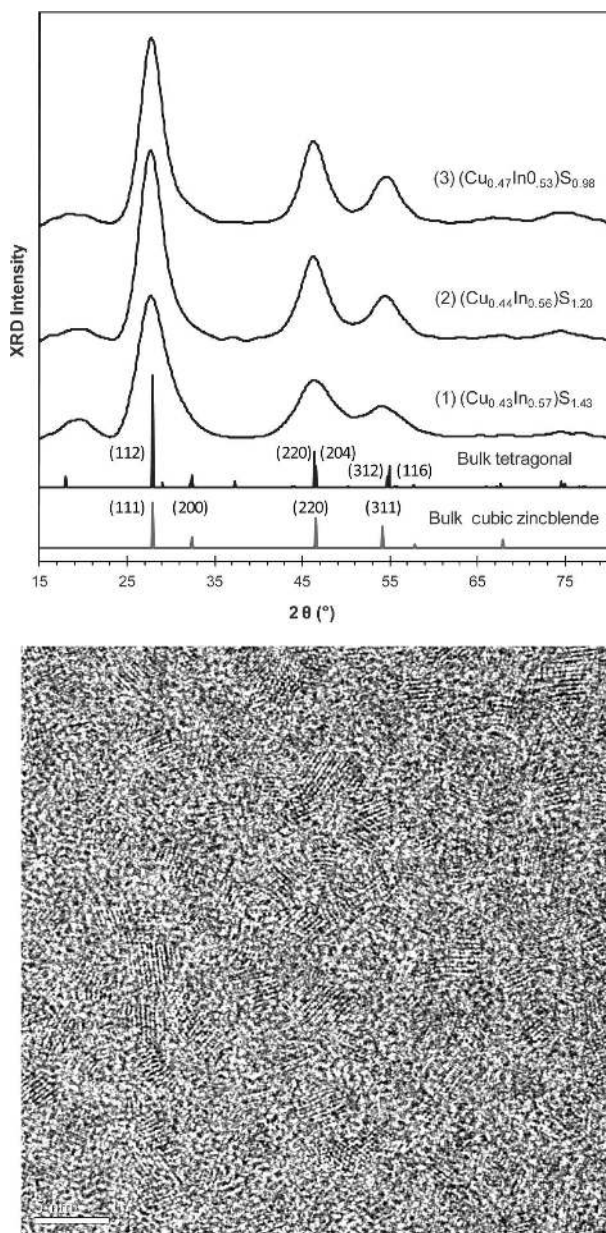
Figure 4. (Top) Powder XRD patterns of the samples taken at 100 °C/15 min (1), 160 °C/15 min (2), and 160 °C/120 min (3), together with that of bulk tetragonal (JCPDS 85-1575) and cubic zincblende $CuInS_2$ as references indexed. The compositions estimated by EDX are indicated. (Bottom) Typical high-resolution TEM image of the 160 °C/120 min $CuInS_2$ NCs; the scale bar is 5 nm.

increase in size. It is well-known that Cu^+ and In^{3+} have similar radii;[13] thus, these three samples exhibited similar diffraction peak positions.

Table 1 summarizes the diameters of the nanocrystals estimated from the diffraction peak (112) of ~2.8 nm (Sample 1), ~3.2 nm (Sample 2), and ~3.4 nm (Sample 3), together with their compositions studied by energy dispersive X-ray spectroscopy (EDX) and X-ray photoelectron spectroscopy (XPS). The three samples exhibited similar EDX $Cu/(Cu + In)$ atomic ratios in the range of 0.45±0.02. Furthermore, such $Cu/(Cu + In)$ atomic ratios obtained from the 1CuI/DDT-to-1In(OAc)$_3$/DDT-to-4SDPP batch also suggest that the overall amount of In is more than that of Cu and support that the reactivity of CuI/DDT is lower than that of In(OAc)$_3$/DDT, in

Table 1. Compositions and Sizes of the Three Samples Shown in Figure 4 XRD Spectra

sample growth	EDX compositions	XPS compositions	XRD mean sizes (nm)
(1) 100 °C/15 min	$Cu_{0.43}In_{0.57}S_{1.43}$	$Cu_{0.21}In_{0.79}S_{1.46}$	2.8
(2) 160 °C/15 min	$Cu_{0.44}In_{0.56}S_{1.20}$	$Cu_{0.30}In_{0.70}S_{1.47}$	3.2
(3) 160 °C/120 min	$Cu_{0.47}In_{0.53}S_{0.98}$	$Cu_{0.30}In_{0.70}S_{1.46}$	3.4

agreement with our ^{31}P NMR (Figure 2) and in situ absorption (Figure 3) measurements.

At the same time, the three samples exhibited XPS $Cu/(Cu + In)$ atomic ratios of 0.21 for Sample 1 and 0.30 for Samples 2 and 3. With EDX more sensitive to bulk and XPS to surface, the larger values of EDX than XPS $Cu/(Cu + In)$ atomic ratios suggest inhomogeneity of the distribution of Cu and In, together with an increase of In from the center of a NC toward the surface. Note that we reported ZnCdS gradiently alloyed NCs with more reactive Cd rich in the inner region of a NC and less reactive Zn rich on the outer region of a NC.[43] Cd is much more reactive than Zn; such an increase in less reactive Zn from the center to the surface is easier to understand. $CuInS_2$ NCs with In rich on their outer region were documented and supported by EDX and XPS.[22] The Cu vacancy has been acknowledged as one of the main defects in $CuInS_2$ NCs.[54,55] The filling of Cu vacancy by In or Zn (through cation exchange) has been employed to achieve higher PL emission QYs; such substitution may widen the band gap at the same time.[22,25] Here, In^{3+} may substitute efficiently the Cu^{1+} vacancy especially on the NC surface because of diffusion during reaction; such a compositional feature of our $CuInS_2$ NCs with the probable gradient distribution of more In^{3+} on the surface rather than Cu^{1+} could be the very reason for the relatively high PL QY.

Figure 4, bottom, demonstrates a typical TEM image of the sample presented in Figure 1. The $CuInS_2$ NCs exhibit high crystallinity with a mean size of 3.4 ± 0.4 nm estimated from the pyramidal shape.[18,56] The composition of this sample was determined by EDX to be $Cu_{0.44}In_{0.56}S_{1.17}$.

For the bright $CuInS_2$ NCs from the eq 1 approach, extensive efforts were carried out, as shown in Figures S3A in the Supporting Information to S3K. See Figure S3A, B in the Supporting Information for the CuI/DDT-to-In(OAc)$_3$/DDT feed molar ratio effect, Figure S3C in the Supporting Information for 1CuI/DDT-to-1In(OAc)$_3$/DDT-to-xSDPP feed molar ratio effect, Figure S3D−F in the Supporting Information for the nature of the reaction medium effect, and Figure S3G−K in the Supporting Information for the effect of the different Cu and In source compounds explored. For the four batches shown in Figure S3B in the Supporting Information with the feed molar ratios of xCuI-(2-x)In-(OAc)$_3$-4SDPP, where x = 1.5, 1, 0.5, and 0.2, Batch 1CuI-1In(OAc)$_3$-4SDPP is superior regarding the quantum yield of the 160 °C/120 min samples. This should be related to the fact that In(OAc)$_3$/DDT is more reactive than CuI/DDT. For the five batches shown in Figure S3C in the Supporting Information with the feed molar ratios of 1CuI-1In(OAc)$_3$-xDPPS, where x = 0.5, 1.2, 2, 4, and 8, again, Batch 1CuI-1In(OAc)$_3$-4SDPP is superior regarding the quantum yield of the 160 °C/120 min samples.

Table 2 summarizes the emission properties of the 160 °C/120 min samples from the six synthetic batches shown in Figure S3D, E in the Supporting Information. With the feed molar

Table 2. Summary of the Emission Properties of the 160 °C/120 min Samples from the Six Flask Reactions Shown in Figure S3D, E in the Supporting Information

reaction media	emission position (nm)	FWHM (nm)	QY (%)
DDT 100	758.8	141.2	15.7
DDT:ODE (76:24)	801.7	148.8	12.3
DDT:ODE (52:48)	815.8	159.0	8.3
DDT:ODE (26:74)	857.8	195.4	2.2
DDT:OA (74:26)	779.9	141.5	11.5
DDT:OLA (76:24)	705.9	115.7	1.7

ratios of 1CuI-to-1In(OAc)$_3$-to-4SDPP, the increase of ODE in DDT led to the decrease of the PL efficiency. Also, the presence of OA or OLA in DDT resulted in the decrease of the PL efficiency. Here OLA may react with SDPP,[37] to solvate the metal reagents,[57] and increase the polarity of the reaction media, leading to delayed nucleation. Therefore, DDT was identified as the sole ligand and solvent to achieve controlled nucleation/growth of CuInS$_2$ NCs. Table 3 summarizes the

Table 3. Summary of the Emission Properties of the 160 °C/120 min Samples from the Nine Flask Reactions Shown in Figure S3G–J in the Supporting Information

Cu source	In source	emission position (nm)	FWHM (nm)	QY (%)
CuI	In(OAc)$_3$	758.8	141.2	16.2
CuCl	In(OAc)$_3$	748.5	156.0	15.9
Cu(OAc)	In(OAc)$_3$	745.2	142.5	12.2
CuBr$_2$	In(OAc)$_3$	824.2	179.7	15.3
CuCl$_2$	In(OAc)$_3$	795.0	176.6	16.6
Cu(OAc)$_2$	In(OAc)$_3$	753.0	142.3	10.5
CuI	In(acac)$_3$	759.0	139.5	17.6
CuI	InCl$_3$	889.9	200.2	0
CuI	InI$_3$	911.5	230.1	0

emission properties of the 160 °C/120 min samples from the nine synthetic batches shown in Figure S3G–J in the Supporting Information. Interestingly, EDX suggested

$(Cu_{0.45}In_{0.55})S_{1.20}$ from Batch 76DDT-to-24ODE (Table 2 with ~13% QY) and $(Cu_{0.46}In_{0.54})S_{1.19}$ from Batch CuI-to-In(acac)$_3$ (Table 3 with ~18% QY). These CuInS$_2$ NCs including those shown in Table 1 exhibit a strong deviation from the ideal 0.5-to-0.5-to-1 chalcopyrite composition; such deviation should have direct consequences on the optical properties of the NCs.

Finally, we applied our CuInS$_2$ NCs for in vitro and in vivo bioimaging applications, based on our previous experience with single-domain antibodies (sdAbs) for selective and efficient cancer detection.[38−41] ZnS coating was performed first and then bio-conjugation with sdAbs EG2 or 2A3. Usually, for a mean size core of ~3.4 nm, its resulting core-shell NC was estimated to be ~6.6 nm leading to the shell thickness of ~1.6 nm. EG2 is a llama sdAb, which was raised against a widely-known tumor marker, epidermal growth factor receptor (EGFR); in the present study, EG2 was used for in vivo brain tumor imaging. 2A3 was derived from a llama sdAb library to target carcinoembryonic antigen-related cell adhesion molecule 6 (CEACAM6), a biomarker of pancreatic cancer; in the present study, 2A3 was used for in vitro pancreatic cancer cell imaging. Figure 5 demonstrates successful bioconjugation, for example, with EG2, via the reduced mobility of bio-conjugated versus non-conjugated CuInS$_2$/ZnS QDs in agarose gel electrophoresis.

See Figure S5 in the Supporting Information for the characterization before and after ZnS coating and subsequent bio-conjugation. For the ZnS coating,[7] a mixture of zinc oleate and zinc ethylxanthate was usually added dropwise to a reaction flask consisting of the CuInS$_2$ NCs at 220 °C. An increase in PL QYs to up to 60 % accompanied by blueshift in emission from ~770 nm to ~710 nm was observed, as shown in Figure S5A in the Supporting Information. The blueshift can be interpreted by a reduction of the core size due to the cation exchange between Zn and Cu/In.[16,22] XRD of the core and core/shell NCs, and bulk CuInS$_2$ and bulk ZnS is shown in Figure S5B in the Supporting Information. The diffraction peak positions of the core/shell NCs locate between those of CuInS$_2$ and ZnS. The EDX compositions of the core and core/shell NCs are
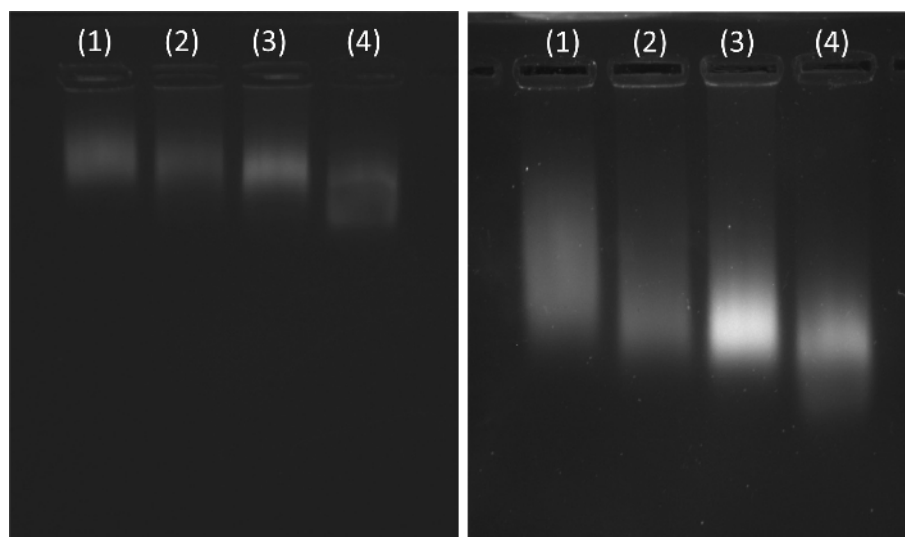

Figure 5. Agarose gel electrophoresis of EG2-CuInS$_2$/ZnS NCs for 20 min (left) and 50 min (right) using Tris-acetate-EDTA (TAE) buffer. Lanes 1−4 are EG2-CuInS$_2$/ZnS NCs purified (1), EG2-PEG-CuInS$_2$/ZnS NCs purified (2), EG2-CuInS$_2$/ZnS unpurified NCs (3), and CuInS$_2$/ZnS NCs (4). The gel images were taken by an eXplore Optix pre-clinical imager at 750 nm.
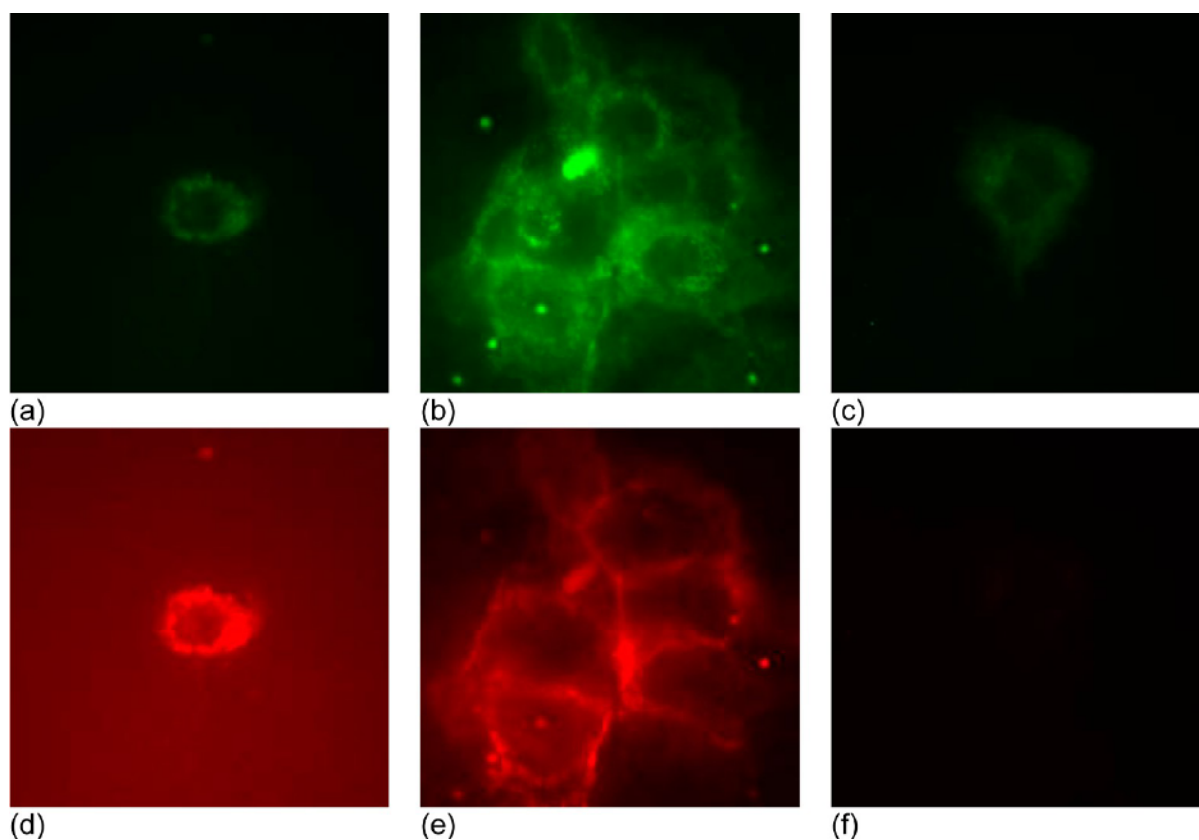
Figure 6. In vitro false color images ($80 \times 80 \ \mu m^2$) of (a−c) autofluorescence excited at 488 nm and detected in the 516−556 nm range, green with the same intensity scale, and (d−f) QD fluorescence excited at 543 nm and detected in the 604−644 nm range, red with the same intensity scale. (a, d) Single BxPC3 pancreatic cancer cell with 2A3-sdAb-CuInS$_2$/ZnS NCs, (b, e) clump of BxPC3 cells with 2A3-sdAb-CuInS$_2$/ZnS NCs, and (c, f) single BxPC3 cell with CuInS$_2$/ZnS NCs. Washing was performed before taking the images. (a−c) Autofluorescence excited at 488 nm (all three images are shown with the same intensity range). (d−f) QD fluorescence excited at 543 nm (all three images are shown with the same intensity range). The images are cropped to an $80 \times 80 \ \mu m^2$ area.

shown in Table S2 in the Supporting Information. Very interestingly, Zn should have replaced In more than Cu, due to the decrease in the In atomic ratio from 0.56 (core NCs) to 0.35 (core−shell NCs). Such Zn replacement of In more than Cu should be related to the gradient structure of the core NCs, which is rich in In on the surface. The TEM image of the core/shell NCs shown in Figure S5B in the Supporting Information demonstrates high crystallinity and low size distribution.

For the bioconjugation, surface ligand exchange was performed first to transfer the CuInS$_2$/ZnS core-shell NCs after purification into aqueous environments. For in vitro imaging of pancreatic cancer cells, dihydrolipoic acid (DHLA) was used for the surface ligand exchange and 2A3 for the bio-conjugation. For in vivo imaging of brain tumor cancer cells, mercaptoundecanoic acid (MUA) was used for the surface ligand exchange and EG2 for the bio-conjugation. The ligand exchange and bioconjugation procedures are illustrated in Figure S5C in the Supporting Information. The EDC method[58] to bioconjugate 2A3 to MUA-capped NCs and EG2 to DHLA-capped NCs was successful. The optical properties of the corresponding QDs used for in vitro imaging (Figure 6) and in vivo imaging (Figure 7) are summarized in Figures S6 and S7 in the Supporting Information, respectively. The QY of our CuInS$_2$/ZnS core−shell NCs decreased from ∼45% to 8% after aqueous phase transfer and bioconjugation; the NCs with ∼8% QY emitting at ∼656 nm and ∼790 nm were sufficiently bright for our bioimaging.
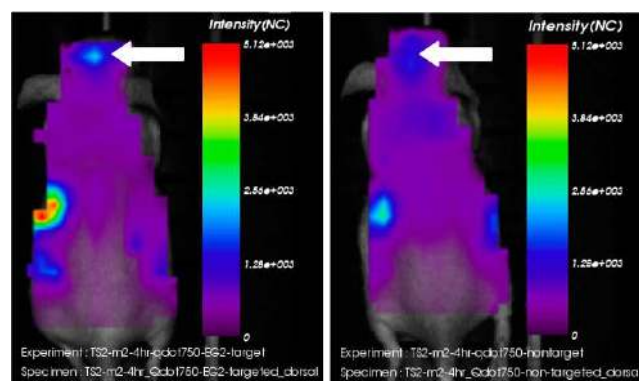

Figure 7. In vivo optical images demonstrate the biodistribution of the EG2 bioconjugated (left) and non-bioconjugated (right) CuInS$_2$/ZnS NCs after their 4 h intravenous injection, as well as enhanced targeting of the bioconjugated CuInS$_2$/ZnS NCs in an orthotopic brain glioblastoma tumor model, as compared by the intensity difference at the two sites pointed by the two arrows. The other bright spots correspond to excretion through the liver.

Figure 6 shows in vitro imaging BxPC3 pancreatic cancer cells with 2A3 bio-conjugated CuInS$_2$/ZnS NCs and non bio-conjugated CuInS$_2$/ZnS NCs. The filter which was used only transmitted the short wavelength tail portion of the luminescence band, the signal-to-noise ratio was sufficiently large to yield images with good contrast. The images shown in

Figure 6 demonstrate that the CuInS$_2$/ZnS NCs without 2A3 are not targeted and are barely detectable (Figure 6f) ,indicating that nonspecific adsorpton is minimal. The intensity of autofluorescence, represented by false-coloured green, is comparable in the top panel images. The intensity of the near-IR fluorescence, signified by false-coloured red, is significantly stronger in images d and e in Figure 6 than in image f, because of the binding of the 2A3 bioconjugated CuInS$_2$/ZnS NCs on the surface of the cancer cells. Thus, the 2A3 conjugation was accomplished and the resulting CuInS$_2$/ZnS NCs have the potential to detect CEACAM6 for the early-stage diagnostics of pancreatic cancer. Note that previously presented western blot data demonstrated that 2A3 binds specifically to cells expressing CEACAM6 and does not bind to CEACAM6-free cells.[41]

Figure 7 shows in vivo imaging brain tumor cancer cells with EG2 bio-conjugated CuInS$_2$/ZnS NCs and non bio-conjugated CuInS$_2$/ZnS NCs. The bioconjugated CuInS$_2$/ZnS NCs were injected into one nude mice nine days after introducing 75,000 U87MG delta EGFR Glioblastoma cells, and the non bioconjugated CuInS$_2$/ZnS NCs were injected into another nude mice as a control. It is clear that, for the mice injected with the bio-conjugated CuInS$_2$/ZnS NCs, the fluorescence intensity at the tumor site is much greater than that of mice injected with the non-bio-conjugated CuInS$_2$/ZnS NCs, and remains at a high level after 4 h of intravenous injection. Note that the intensity scale is logarithmic. The region with bright signal in the dorsal side of the mouse corresponds to the liver of the mouse. Liver is a major organ of the reticulo-endothelial system. Many of the NCs end up in the liver, leading to the high fluorescent signal. The difference in brightness of the liver region in the two figures may be due to different clearance and pharmacokinetics of the NCs when they are bio-conjugated or not to the sdAb. Thus, the EG2 conjugation was successful and the resulting CuInS$_2$/ZnS NCs are unambiguously capable of in vivo imaging in the near IR window.

3. CONCLUSIONS

Diphenylphosphine sulfide (SDPP) was used as a sulphur source to synthesize brightly-emissive CuInS$_2$ NCs via a low-temperature non-injection one-pot approach in 1-dodecanethiol (DDT), which is the sole ligand and solvent. The low nucleation/growth temperature is due to the high reactivity of SDPP. At the same time, the relatively low CuI/DDT reactivity as compared to that of In(OAc)$_3$/DDT results in a gradient structure with an In-rich surface; thus, the resulting CuInS$_2$ NCs exhibited high QY of 23%. The exploration of the chemical mechanism of the SDPP and SeDPP based approaches to QDs is an ongoing effort in our laboratories.[66] An enhanced QY to 50−60% was achieved via ZnS shell coating; the resulting core-shell NCs were transferred into aqueous phases for the subsequent bio-conjugation with sdAbs. In vitro pancreatic cancer cell imaging was performed, together with in vivo brain tumor targeted imaging, demonstrating high specificity of cancer targeting with high detection sensitivity.

4. EXPERIMENTAL SECTION

4.1. Chemicals. All chemicals used are commercially available and were used as received. Copper(I) iodide (CuI, 98%), copper(I) chloride (CuCl, 99.995+%), copper(I) bromide (CuBr, 98%), copper(I) acetate (Cu(OAc), 97%), indium(III) acetate (In(OAc)$_3$, 99.99%), indium(III) chloride (InCl$_3$, 98%), zinc acetate dihydrate (Zn(OAc)$_2$·H$_2$O, 99.999%), zinc chloride (ZnCl$_2$, 99.999%),

potassium ethyl xanthogenate (96%), 1-dodecanethiol (DDT, 98%), oleic acid (OA, tech. 90%), oleylamine (OLA, tech. 70%), 1-octadecene (ODE, tech. 90%), mercaptoundecanoic acid (MUA, 98%), tetramethyl ammonium hydroxide (TMAH, 25 wt % in H$_2$O), 1-ethyl-3-[3-dimethylaminopropyl]carbodiimide (EDC), N,N'-dicyclohexylcarbodiimide (DCC, 99%), N-hydroxysuccinimide (NHS) were purchased from Sigma-Aldrich. Diphenylphosphine (DPP, 99%), copper(II) bromide (CuBr$_2$, 99%), copper(II) chloride (CuCl$_2$, anhydrous, 98%), copper(II) acetate (Cu(OAc)$_2$, anhydrous, 97%), indium(III) iodide (InI$_3$, 99.999%) and indium(III) acetylacetonate (In(acac)$_3$, 98%) were purchased from Strem Chemicals. Sulfur (precipitated) was purchased from Anachemia. Solvents used for purification were anhydrous, including toluene (99.8 %), hexane (≥99 %), and methanol (99.8 %), which were purchased from Sigma-Aldrich, along with acetone (99.5 %, ACP in Montreal, dried over 4 Å molecular sieves).

4.2. Synthesis of CuInS$_2$ NCs. The SDPP stock solution (0.66 M) was prepared in a glovebox by adding DPP (1.6 mL, 9.1 mmol) to a vial containing sulphur (0.289 g, 9.0 mmol). The resulting mixture was gently heated with the cap sealed until a clear, colorless solution was obtained, and then was allowed to cool, whereupon a white solid appeared. Toluene (12.0 mL) was then added, and the mixture was gently heated until a clear, colorless solution was obtained.

In a typical synthesis of CuInS$_2$ NCs, CuI (0.20 mmol, 38 mg) and In(OAc)$_3$ (0.20 mmol, 58 mg) were added to a three-neck round-bottom flask equipped with a condenser, thermometer, and magnetic stir bar. DDT (6.25 mL) was added with rigorous stirring, and then degassed at room temperature. When vigorous bubbling subsided, the temperature was increased to 65 °C and degassed further for 1 h. If a clear, yellow solution was not observed, the mixture was heated at 120 °C under N$_2$ until this was obtained, and then degassed again at 60 °C for 1 h. The temperature was lowered to 50 °C and the DPPS stock solution (1.07 mL, 0.71 mmol) was added under N$_2$. The reaction was then degassed once more for 0.5 h to remove toluene. Under a flow of purified N$_2$, the reaction mixture was heated up from 50 °C to 160 °C in a stepwise manner. To monitor the growth kinetics, 11 samples (∼100 μL each) were taken with their temperature/growth periods of 50 °C/30 min (1), 60 °C/15 min (2), 80 °C/15 min (3), 100 °C/15 min (4), 120 °C/15 min (5), 140 °C/15 min (6), 160 °C/15 min (7), 160 °C/30 min (8), 160 °C/60 min (9), 160 °C/90 min (10), 160 °C/120 min (11). In some cases, 10 samples were collected without the sampling at 160 °C/90 min. The absorption and PL emission (excited at 500 nm) spectra were collected with diluted samples, which included 5 μL of crude growth mixtures dispersed in 1 mL toluene.

4.3. ^{31}P NMR with ^{1}H Decoupling. The measurements were performed on a Bruker AV-III 400 spectrometer operating at 161.98 MHz for ^{31}P. An external standard 85% H$_3$PO$_4$ was used.

CuI-DDT stock solution (75 mmol/kg) was made from CuI (76 mg, 0.4 mmol) and DDT (6.25 mL), whereas In(OAc)$_3$-DDT stock solution (25 mmol/kg) was made from In(OAc)$_3$ (58 mg, 0.2 mmol) and DDT (9.38 mL). The mixtures were degassed separately at 60−70 °C till a clear solution was obtained and then transferred into a glovebox filled with N$_2$. DPPS stock solution in toluene-d$_8$ (0.66 M) was prepared in a similar manner as that in toluene by mixing S (48 mg, 1.5 mmol) and DPP (0.26 mL, 1.5 mmol) in toluene-d$_8$ (2.0 mL).

For the top NMR spectra in Figure 2, 0.48 mL (0.03 mmol) of CuI-DDT stock solution was added into a 5 mm NMR tube, followed by 0.08 mL (0.053 mmol) of DPPS stock solution, leading to [Cu] of ∼74 mmol/kg. For the middle NMR spectra in Figure 2, 1.95 g of (0.05 mmol) In(OAc)$_3$-DDT stock solution was added into a 10 mm NMR tube, followed by 0.13 mL (0.09 mmol) of DPPS stock solution, leading to [In] ∼21 mmol/kg. For the bottom NMR spectra in Figure 2, 0.30 mL (0.02 mmol) of CuI-DDT stock solution was added to a 5 mm NMR tube, followed by 0.76 g (0.02 mmol) of In(OAc)$_3$-DDT stock solution and 0.10 mL (0.066 mmol) of DPPS stock solution, leading to [Cu + In] of ∼38 mmol/kg. All the samples were prepared in the glovebox filled with N$_2$.

4.4. In situ Observation of the Temporal Evolution of Absorption. All the absorption spectra were collected on a Cary 5000 UV/VIS/NIR spectrometer using a 1 nm data interval and a scan rate

of 600 nm/min. The reaction mixtures were loaded in 3.5 mL cuvettes and the growth time started to count after the cuvettes were placed in the instrument with the set up of reaction temperature and spectra collecting time intervals. The light path was 10 mm.

4.5. ZnS Shell Coating. The zinc oleate stock solution (0.25 mmol/g) was prepared by mixing $Zn(OAc)_2 \cdot 2H_2O$ (2.19 g, 10.0 mmol), oleic acid (6.21 g, 22.0 mmol), and ODE (33 g) in a 100 mL three-neck round-bottom flask equipped with a condenser and thermometer. The mixture was gradually heated to ~100 °C with stirring under vacuum until no vigorous bubbling was observed. The temperature was increased to 140 °C under N_2 until a clear solution was obtained. The temperature was decreased to ~100 °C and degassed once more for ~1 h. At this point, the reaction was allowed to cool to room temperature under N_2.

Shell coating of the $CuInS_2$ NCs with ZnS was carried out in situ without purification of the core, following literature procedures.[7] A portion of the CIS core material (~0.10 mmol) was degassed at 60 °C for 1 h in a three-neck round-bottom flask with a condenser. In a separate reaction vessel, the zinc oleate stock solution (0.84 mmol, 3.36 g) was degassed at ~90 °C for 1 h, and a solution of zinc ethylxanthate (0.10 mmol, $Zn(ex)_2$, prepared from $ZnCl_2$ and potassium ethyl xanthogenate.[59]) in 0.10 mL of dimethylformamide (DMF) and 1.0 mL of toluene was added with stirring, forming the ZnS precursor solution. The core material mixture was heated to 220 °C under N_2, and the ZnS precursor solution was added dropwise over 30 min (addition was performed over 45 min for larger batches). After the addition was complete, the reaction was heated for a further 10 min then cooled to room temperature. The core synthesis and shell coating have both been successfully scaled up by a factor of five by volume without a significant decline in optical properties.

4.6. Characterization. Absorption spectra were collected with a Cary 500 UV-vis-NIR spectrophotometer. PL emission spectra were collected with a Horiba Jobin Yvon FluoroMax-4 NIR spectrofluorometer. Both optical measurements used a 1 nm data interval. Built-in Origin 8 was used for the integration of emission peaks to determine peak positions, fwhm, and areas. The PL QY was estimated by comparing the emission intensity of dilute samples in toluene (optical density of ~0.1 at the excitation wavelength of 500 nm) with that of oxazine 170 (lit. QY 60%) in ethanol.[42] The difference of the refractive index of the two solvents was corrected for the QY estimation.

Prior to following characterizations, intensive purification was done for samples. Purification was carried out by dispersing the crude mixture in toluene and methanol (~1:1:1 by volume), followed by centrifugation (6000 rpm for 12 min). After removal of the supernatant, the remaining solids were dispersed in a minimum amount of hexane. The dispersion was centrifuged to remove insoluble particles and transferred to a clean centrifuge tube. Acetone was added to this dispersion to induce precipitation of the NCs, and was then separated by centrifugation. The supernatant was removed and the remaining crystals were dried under a N_2 stream.

Powder X-ray diffraction (XRD) patterns were recorded at room temperature on a Bruker Axs D8 X-ray diffractometer using Cu Kα radiation in a θ−θ mode. The generator was operated at 40 kV and 40 mA. Data were collected in a range between 15 and 80° (2θ) with a step size of 0.1° and a counting time of 7 s per step. An XRD sample was prepared by depositing a concentrated NC dispersion in hexane on a low background quartz plate.

Transmission electron microscopy (TEM) samples were prepared by depositing diluted NC dispersions in hexane onto 400-mesh thin-carbon-coated Cu grids, followed by drying in air. The samples were examined in a JEOL JEM-2100F electron microscope equipped with a scanning unit (STEM) operating at 200 kV. High resolution TEM (HRTEM) images were obtained using a Gatan UltraScan 1000 CCD camera, and high angle annular dark field scanning TEM (HAADF-STEM) images were obtained using a Gatan ADF detector. The NC sizes were obtained by manually analyzing ~100 individual NCs. The atomic composition of the NCs was studied by the energy dispersive X-ray spectroscopy (EDX) in the STEM mode using an Oxford INCA Energy TEM 200 attached to the JEM-2100F. The EDX samples were

prepared by concentrated NC dispersions in hexane deposited onto 300-mesh thin-carbon-coated Mo grids, followed by drying in air.

X-ray photoelectron spectroscopy (XPS) was performed using a Kratos Axis Ultra XPS equipped with a monochromated Al Kα X-ray source. The instrument pressure in the analysis chamber was 2.0×10^{-9} Torr during analysis. Survey scans were conducted using a pass energy of 160 eV, while high resolution scans were carried out at 20 eV using an analysis area of approximately 300×700 μm^2. Peak fitting was performed using CasaXPS (ver. 2.2.107) data processing software. Shirley background correction procedures were used as provided by CasaXPS. Curve fitting procedures used for high resolution spectra presented in this report employed a Gaussian-Lorentzian function. High resolution analyses were calibrated to adventitious C 1s signal, at 285 eV. Quantification was performed using sensitivity factors provided by CasaXPS's Scofield element library.

4.7. Surface Ligand Exchange. Ligand exchange was performed with purified $CuInS_2/ZnS$ core−shell NCs. For in vitro imaging, dihydrolipoic acid (DHLA, 208 mg, 1 mmol, prepared following literature method[60]) was dissolved in 2 mL of methanol containing ~80 mg of NaOH. To this solution, ~70 mg of $Zn(NO_3)_2 \bullet 6H_2O$ (0.24 mmol) was added and the mixture was stirred vigorously until a clear solution was obtained. To 2 mL of such a solution was added 0.1 mL of a $CuInS_2/ZnS$ stock solution, which was prepared by adding 2 mL dry toluene to ~40 mg of the purified NCs, and the mixture was stirred at room temperature for 24 h and then centrifuged (4000 rpm/ 30 min). The precipitates were washed with ~500 μL methanol (precipitates were partially dissolved in methanol) and then centrifuged again. Precipitates were dispersed in water and filtered using 0.45 μm and 0.22 μm pore size syringe filters (some QDs may not be filtered out).

For in vivo imaging, MUA (0.93 g, 4.3 mmol) was added to 10 mL of methanol and shaken vigorously. Tetramethyl ammonium hydroxide (TMAH) was slowly added until a pH of 9−10 was attained, and then this solution was stirred for 1 h. A portion of this basic solution (3 mL) was added to 0.1 mL of a $CuInS_2/ZnS$ stock solution, which was prepared by adding 2 mL of dry toluene to ~40 mg of the purified NCs. The reaction was stirred vigorously for 3−24 h and monitored by observing the amounts of precipitate in the vessel. At the end of the reaction, the mixture was centrifuged and the supernatant was decanted. Chloroform was added to the decanted supernatant and the aqueous and organic phases were separated after shaking thoroughly.

4.8. Bioconjugation. The purified $CuInS_2/ZnS$ QDs were bioconjugated with sdAbs 2A3 and EG2 for in vitro and in vivo imaging, respectively. For in vitro imaging, the DHLA-capped $CuInS_2/ZnS$ stock solution (~1×10^{-5} mmol) was mixed with a PBS solution consisting of sdAb 2A3 (2.5 mg/mL sdAb/PBS), where 2A3 is estimated to be ~1×10^{-5} mmol based on a molecular weight of ~15 K. Then 20 mL (~1×10^{-4} mmol) of EDC and 10 mL (~1×10^{-4} mmol) of NHS were added at room temperature and the mixture was stirred vigorously for no more than 1h. The resulting bioconjugates, unpurified and purified, were used for biological applications. The purification was carried out with a 30,000 MWCO centrifuge filter device. The feed molar ratio of QD:sdAb is 1:1, so the purified bioconjugates should have a molecular weight greater than 30 kDa. Only the bioconjugates and not the reactants should be retained on the filter used.

For in vivo imaging, the MUA-capped $CuInS_2/ZnS$ NC stock solution (0.4 mL, ~4×10^{-5} mmol) was mixed with 0.4 mL of a PBS solution containing the sdAb EG2 (2.5 mg/mL EG2/PBS). To this was added EDC (0.020 mL, ~1×10^{-4} mmol) and NHS (0.010 mL, ~1×10^{-4} mmol), and the resulting mixture was stirred vigorously for 1 h. The resulting bioconjugates, both purified and unpurified, were used for the bioimaging. The purification was carried out with a 30 000 MWCO centrifuge filter device, as above.

4.9. Gel Electrophoresis. 1% Ultra Pure Agarose (Invitrogen) gel was used. Once the gel was solidified, the samples were loaded on the gel and the electrophoresis was performed for 20 and 50 min using a Tris-acetate-EDTA (TAE) buffer. Afterwards the samples were visualized by using eXplore Optix pre-clinical imager at 750 nm.

4.10. In vitro Imaging. The BxPC3 human pancreatic cancer cell line was used, which was obtained from American Type Culture Collection (ATCC). The cells were cultured in RPMI (Gibco) medium supplemented with 10% fetal bovine serum (Roche) at 37 °C, 5% CO_2 in 6-well plates (Falcon) with a sterile coverslip in each well. When the cells were about 70% confluence by the next day, they were fixed on the coverslips by using 10% formaldehyde in PBS for 10 minutes. Then, cells were washed three times with PBS and then incubated with 2% skimmed milk in PBS for 2 h. After washing with PBS, cells were incubated with 2A3 conjugated or unconjugated $CuInS_2$/ZnS NCs for 1 h and washed three times with PBS. It is important to note that the cells were washed after labeling so that unconjugated QDs that were not targeted to the cells are washed off. Two sets of fluorescence images were recorded for each sample with an Olympus IX-81 fluorescence microscope equipped with Photo-metrics Cascade 512B EMCCD camera. The images were acquired using a 60x oil immersion objective and the same excitation and detection conditions were applied for each set. In the first set, the samples were excited at 488 nm and weak autofluorescence was detected in the 516−556 nm range (Figure 6 top). In the second set, the samples were excited at 543 nm (Figure 6 bottom). The samples treated with 2A3 conjugated CuInS2/ZnS QDs showed strong fluorescence signal in the 604-644 nm range, whereas no fluorescence was observed for the samples treated with unconjugated CuInS2/ZnS. Similarly, no fluorescence was observed in the 604-664 nm range for untreated cells upon irradiation at 543 nm. Typical images are shown in Figure 6 and presented with false color, the 488 nm excitation images in green and the 543 nm excitation images in red. The same color images are presented using the same intensity scale to facilitate fluorescence intensity comparison between 2A3 conjugated and unconjugated samples.

4.11. In vivo Imaging. Firstly, intracranial models of U87MG.EGFRvIII glioblastoma in nude mice were used. All animal procedures were approved by the NRC-IBS Animal Care Committee and were in compliance with the Canadian Council of Animal Care. CD-1 nude mice (males, 6−8 weeks old) were purchased from Charles River Canada. The animals were housed in cages, maintained on a 12 h light/dark schedule at a temperature of 22 °C and a relative humidity of 50 ± 5%. Food and water was available ad libitum. U87MG.EGFRvIII carrying the deletion mutant of EGFR (EGFRvIII) cells was cultured in DMEM supplemented with 10% fetal calf serum and maintained in a humidified 5% CO_2 atmosphere at 37 °C. This EGFRvIII mutation confers enhanced tumorgenicity in vivo,[61] and there is differential expression of the EGFR protein compared to the U87MG parental cell line.[62] Cells were harvested by trypsinization in EDTA/trypsin, washed in PBS, and centrifuged three times at 200 g for 2 min. Cell number was determined and mice were anesthetized with isofluorane anesthesia and the scalp was swabbed with alcohol. The skin was incised and a 10 μL Hamilton syringe was used to inoculate a 5 μL cell suspension (75000 cells) into the corpus striatum in the left hemisphere (3.0 mm deep; 1 mm anterior and 2.0 mm lateral to the bregma). The U87MG.EGFRvIII implanted tumors were allowed to grow for 9 days before the beginning of imaging experiments.

Secondly, in vivo brain tumor fluorescence imaging was carried out with near-infrared $CuInS_2$/ZnS NCs bioconjugated with sdAb EG2 as targeted NCs and $CuInS_2$/ZnS as non-targeted NCs. Mice bearing 9 day old U87MG.EGFRvIII intracranial brain tumors were injected with QD via the tail vein (20 μL of 1 μM solution). Animals were subjected to in vivo imaging studies using a small-animal time-domain eXplore Optix MX2 preclinical imager (Advanced Research Technologies, Montreal, QC, Canada), as described previously.[63−65] In all imaging experiments, a 488 nm pulsed laser diode was used for excitation, and the fluorescence emission was collected at 750 nm. Each animal was imaged whole body at various time points after i.v. injection. The data were recorded as temporal point-spread functions (TPSF) and the images were reconstructed as fluorescence concentration maps. Total fluorescence intensity data from ROIs placed around the tumor region, were subsequently analyzed using the

OptiView software package (Advanced Research Technologies, Montreal, QC, Canada).

ASSOCIATED CONTENT

ⓈSupporting Information
Additional ^{31}P NMR spectra, XRD patterns, TEM images, absorption and PL spectra of the $CuInS_2$ nanocrystals. This material is available free of charge via the Internet at http://pubs.acs.org.

AUTHOR INFORMATION

Corresponding Author
*Phone: 1-(613)-993-5265; 1-(613)-993-9273. E-mail: Dennis.Whitfield@nrc-cnrc.gc.ca (D.M.W.); kui.yu@nrc.ca (K.Y.). Fax: 1-(613)-998-7833.

Present Address
§M.B.Z. is at Advanced Medical Research Institute of Canada, Division of Medical Sciences, Northern Ontario School of Medicine, Laurentian University, Health Science North, 41 Ramsey Lake Road, Sudbury, Ontario, Canada P3E 5J1.

Notes
The authors declare no competing financial interest.

ACKNOWLEDGMENTS

REFERENCES

(1) Tan, Z.; Zhang, Y.; Xie, C.; Su, H.; Liu, J.; Zhang, C.; Dellas, N.; Mohney, S. E.; Wang, Y.; Wang, J.; Xu, J. Adv. Mater. **2011**, 23, 3553−3558.
(2) Zhang, Y.; Xie, C.; Su, H.; Liu, J.; Pickering, S.; Wang, Y.; Yu, W. W.; Wang, J.; Wang, Y.; Hahm, J.; Dellas, N.; Mohney, S. E.; Xu, J. Nano Lett. **2011**, 11, 329−332.
(3) Song, W.-S.; Yang, H. Chem. Mater. **2012**, 24, 1961−1967.
(4) Li, L.; Coates, N.; Moses, D. J. Am. Chem. Soc. **2010**, 132, 22−23.
(5) Liu, W.; Mitzi, D. B.; Yuan, M.; Kellock, A. J.; Chey, S. J.; Gunawan, O. Chem. Mater. **2010**, 22, 1010−1014.
(6) Weil, B. D.; Connor, S. T.; Cui, Y. J. Am. Chem. Soc. **2010**, 132, 6642−6643.
(7) Li, L.; Daou, T. J.; Texier, I.; Kim Chi, T. T.; Liem, H. Q.; Reiss, P. Chem. Mater. **2009**, 21, 2422−2429.
(8) Pons, T.; Pic, E.; Lequeux, N.; Cassette, E.; Bezdetnaya, L.; Guillemin, F.; Marchal, F.; Dubertret, B. ACS Nano **2010**, 4, 2531−2538.

(9) Yong, K.-T.; Roy, I.; Hu, R.; Ding, H.; Cai, H.; Zhu, J.; Zhang, X.; Bergeya, E. J.; Prasad, P. N. *Integr. Biol.* **2010**, *2*, 121−129.

(10) Tang, X.; Cheng, W.; Choo, E. S. G.; Xue, J. *Chem. Commun.* **2011**, *47*, 5217−5219.

(11) Hsu, J.-C.; Huang, C.-C.; Ou, K.-L.; Lu, N.; Mai, F.-D.; Chen, J.-K.; Chang, J.-Y. *J. Mater. Chem.* **2011**, *21*, 19257−19266.

(12) Deng, D.; Chen, Y.; Cao, J.; Tian, J.; Qian, Z.; Achilefu, S.; Gu, Y. *Chem. Mater.* **2012**, *24*, 3029−3037.

(13) Pan, D.; An, L.; Sun, Z.; Hou, W.; Yang, Y.; Yang, Z.; Lu, Y. *J. Am. Chem. Soc.* **2008**, *130*, 5620−5621.

(14) Xie, R.; Rutherford, M.; Peng, X. *J. Am. Chem. Soc.* **2009**, *131*, 5691−5697.

(15) Kruszynska, M.; Borchert, H.; Parisi, J.; Kolny-Olesiak, J. *J. Am. Chem. Soc.* **2010**, *132*, 15976−15986.

(16) Park, J.; Kim, S.-W. *J. Mater. Chem.* **2011**, *21*, 3745−3750.

(17) Zhong, H.; Zhou, Y.; Ye, M.; He, Y.; Ye, J.; He, C.; Yang, C.; Li, Y. *Chem. Mater.* **2008**, *20*, 6434−6443.

(18) Zhong, H.; Lo, S. S.; Mirkovic, T.; Li, Y.; Ding, Y.; Li, Y.; Scholes, G. D. *ACS Nano* **2010**, *4*, 5253−5262.

(19) Li, L.; Pandey, A.; Werder, D. J.; Khanal, B. P.; Pietryga, J. M.; Klimov, V. I. *J. Am. Chem. Soc.* **2011**, *133*, 1176−1179.

(20) Nam, D.-E.; Song, W.-S.; Yang, H. *J. Colloid. Interface. Sci.* **2011**, *361*, 491−496.

(21) Lu, X.; Zhuang, Z.; Peng, Q.; Li, Y. *CrystEngComm* **2011**, *13*, 4039−4045.

(22) Trizio, L. D.; Prato, M.; Genovese, A.; Casu, A.; Povia, M.; Simonutti, R.; Alcocer, M. J. P.; D'Andrea, C.; Tassone, F.; Manna, L. *Chem. Mater.* **2012**, *24*, 2400−2406.

(23) Li, T.-L.; Teng, H. *J. Mater. Chem.* **2010**, *20*, 3656−3664.

(24) Niezgoda, J. S.; Harrison, M. A.; McBride, J. R.; Rosenthal, S. J. *Chem. Mater.* **2012**, *24*, 3294−3298.

(25) Chen, B.; Zhong, H.; Zhang, W.; Tan, Z.; Li, Y.; Yu, C.; Zhai, T.; Bando, Y.; Yang, S.; Zou, B. *Adv. Funct. Mater.* **2012**, *22*, 2081−2088.

(26) Ouyang, J.; Schuurmans, C.; Zhang, Y.; Nagelkerke, R.; Wu, X.; Kingston, D.; Wang, Z. Y.; Wilkinson, D.; Li, C.; Leek, D. M.; Tao, Y.; Yu, K. *ACS Appl. Mater. Interfaces* **2011**, *3*, 553−565.

(27) Steckel, J. S.; Yen, B. K. H.; Oertel, D. C.; Bawendi, M. G. *J. Am. Chem. Soc.* **2006**, *128*, 13032−13033.

(28) Joo, J.; Pietryga, J. M.; McGuire, J. A.; Jeon, S.-H.; Williams, D. J.; Wang, H.-L.; Klimov, V. I. *J. Am. Chem. Soc.* **2009**, *131*, 10620−10628.

(29) Evans, C. M.; Evans, M. E.; Krauss, T. D. *J. Am. Chem. Soc.* **2010**, *132*, 10973−10975.

(30) Yu, K.; Ouyang, J.; Zhang, Y.; Tung, H. T.; Lin, S.; Nagelkerke, R.; Kingston, D.; Wu, X.; Leek, M. D.; Wilkinson, D.; Li, C.; Chen, I. G.; Tao, Y. *ACS Appl. Mater. Interfaces* **2011**, *3*, 1511−1520.

(31) Ma, W.; Luther, J. M.; Zheng, H.; Wu, Y.; Alivisatos, A. P. *Nano Lett.* **2009**, *9*, 1699−1703.

(32) Smith, D. K.; Luther, J. M.; Semonin, O. E.; Nozik, A. J.; Beard, M. C. *ACS Nano* **2011**, *5*, 183−190.

(33) Yu, K.; Hrdina, A.; Zhang, X.; Ouyang, J.; Leek, D. M.; Wu, X.; Gong, M.; Wilkinson, D.; Li, C. *Chem. Commun.* **2011**, *47*, 8811−8813.

(34) Yu, K.; Hrdina, A.; Ouyang, J.; Kingston, D.; Wu, X.; Leek, D. M.; Liu, X.; Li, C. *ACS Appl. Mater. Interfaces* **2012**, *4*, 4302−4311.

(35) Wei, H. H.-Y.; Evans, C. M.; Swartz, B. D.; Neukirch, A. J.; Young, J.; Prezhdo, O. V.; Krauss, T. D. *Nano Lett.* **2012**, *12*, 4465−4471.

(36) Yu, K. *Adv. Mater.* **2012**, *24*, 1123−1132.

(37) Cossairt, B. M.; Owen, J. S. *Chem. Mater.* **2011**, *23*, 3114−3119.

(38) Zaman, M. B.; Baral, T. N.; Zhang, J.; Whitfield, D.; Yu, K. *J. Phys. Chem. C* **2009**, *113*, 496−499.

(39) Zaman, M. B.; Baral, T. N.; Jakubek, Z. J.; Zhang, J.; Wu, X.; Lai, E.; Whitfield, D.; Yu, K. *J. Nanosci. Nanotechnol.* **2011**, *11*, 3757−63.

(40) Baral, T. N.; Murad, Y.; Nguyen, T. D.; Iqbal, U.; Zhang, J. *J. Immunol. Methods* **2011**, *371*, 70−80.

(41) Cheng, T. M.; Murad, Y. M.; Chang, C. C.; Yang, M. C.; Baral, T. N.; Cowan, A.; Tseng, S. H.; Wong, A.; MacKenzie, R.; Zhang, J. *Eur. J. Cancer* **2012**, DOI: 10.1016/j.ejca.2012.07.019.

(42) Sens, R.; Drexhage, K. H. *J. Lumin.* **1981**, *24−25*, 709−712.

(43) Ouyang, J.; Ratcliffe, C. I.; Kingston, D.; Wilkinson, B.; Kuijper, J.; Wu, X.; Ripmeester, J. A.; Yu, K. *J. Phys. Chem. C* **2008**, *112*, 4908−4909.

(44) Yu, K.; Zaman, M. B.; Romanova, S.; Wang, D. S.; Ripmeester, J. A. *Small* **2005**, *1*, 332−338.

(45) Peters, G. *J. Org. Chem.* **1962**, *27*, 2198−2201.

(46) Pilkington, M. J.; Slawin, A. M. Z.; Williams, D. J.; Woollings, J. D. *Main Group Chem.* **1995**, *1*, 145−151.

(47) Cain, M. F.; Hughes, R. P.; Glueck, D. S.; Golen, J. A.; Moore, C. E.; Rheingold, A. L. *Inorg. Chem.* **2010**, *49*, 7650−7662.

(48) Lemmen, T. H.; Goeden, G. V.; Huffman, J. C.; Geerst, R. L.; Caulton, K. G. *Inorg. Chem.* **1990**, *29*, 3680−3685.

(49) McCleverty, J. A.; Kowalski, R. S. Z.; Bailey, N. A.; Mulvaney, R.; O'Cleirigh, D. A. *J. Chem. Soc., Dalton Trans.* **1983**, 627−634.

(50) Casas, J. S.; García-Tasende, M. S.; Sánchez, A.; Sordo, J.; Vázquez-López, E. M. *Inorganica Chimica Acta* **1994**, *219*, 115−119.

(51) Zukerman-Schpector, J.; Haiduc, I. *Polyhedron* **1995**, *14*, 3087−3094.

(52) Our unpublished ^{31}P NMR data.

(53) Pearson, R. G. *J. Am. Chem. Soc.* **1963**, *85*, 3533−3539.

(54) Castro, S. L.; Bailey, S. G.; Banger, K. K.; Hepp, A. F. *J. Phys. Chem. B* **2004**, *108*, 12429−12434.

(55) Uehara, M.; Watanabe, K.; Tajiri, Y.; Nakamura, H.; Maeda, H. *J. Chem. Phys.* **2008**, *129*, 134709.

(56) Booth, M.; Brown, A. P.; Evans, S. D.; Critchley, K. *Chem. Mater.* **2012**, *24*, 2064−2070.

(57) Allen, P. M.; Walker, B. J.; Bawendi, M. G. *Angew. Chem., Int. Ed.* **2010**, *49*, 760−762.

(58) Hermanson, G. T. *Bioconjugate Techniques*, 2nd ed.; Elsevier Science: San Diego, CA, 2008; pp 216−223.

(59) Protière, M.; Reiss, P. *Small* **2007**, *3*, 399−403.

(60) Gunsalus, I. C.; Barton, L. S.; Gruber, W. *J. Am. Chem. Soc.* **1956**, *78*, 1763−1768.

(61) Cheng, S. Y.; Huang, H. J.; Nagane, M.; Ji, X. D.; Wang, D.; Shih, C.C.-Y.; Arap, W.; Huang, , C. M.; Cavenee, W. K. *Proc. Natl. Acad. Sci. U.S.A.* **1996**, *93*, 8502−8507.

(62) Zhang, R.; Tremblay, T. L.; McDermid, A.; Thibault, P.; Stanimirovic, D. *Glia* **2003**, *42*, 194−208.

(63) Abulrob, A.; Brunette, E.; Slinn, J.; Baumann, E.; Stanimirovic, D. *Mol. Imaging* **2007**, *6*, 304−314.

(64) Abulrob, A.; Brunette, E.; Slinn, J.; Baumann, E.; Stanimirovic, D. *Mol. Imaging* **2008**, *7*, 248−262.

(65) Iqbal, U.; Albaghdadi, H.; Luo, Y.; Arbabi, M.; Desvaux, C.; Veres, T.; Stanimirovic, D.; Abulrob, A. *Br. J. Cancer.* **2010**, *103*, 1606−1616.

(66) Yu, K.; Liu, X.; Zeng, Q.; Leek , D. M.; Ouyang, J.; Whitmore, K. M.; Ripmeester, J. A.; Tao, Y.; Yang, M. *Angew. Chem.* **2013**, *52*, DOI: 10.1002/ange.201300568.